PERGAMON

International Journal of Solids and Structures 39 (2002) 4215–4235

INTERNATIONAL JOURNAL OF SOLIDS and STRUCTURES

www.elsevier.com/locate/ijsolstr

Impact failure characteristics in sandwich structures Part I: Basic failure mode selection

L. Roy Xu [a], Ares J. Rosakis [b,*]

[a] Department of Civil and Environmental Engineering, Station B 351831, Vanderbilt University, Nashville, TN 37235, USA
[b] Graduate Aeronautical Laboratories, California Institute of Technology, Mail Stop 105-50, Pasadena, CA 91125, USA

Received 25 July 2001; received in revised form 27 February 2002

Abstract

In the present work we present a systematic experimental investigation of the generation and subsequent evolution of dynamic failure modes in sandwich structures subjected to low-speed impact. Model sandwich specimens involving a compliant polymer core sandwiched between two metal layers were designed and subjected to impact loading to simulate failure evolution mechanisms in real sandwich structures. High-speed photography and dynamic photoelasticity were utilized to study the nature and sequence of such failure modes. A series of complex failure modes was documented. In all cases, inter-layer (interfacial) cracks appeared first. These cracks were shear-dominated and were often intersonic even under moderate impact speeds. The transition from inter-layer crack growth to intra-layer crack formation was also observed. The shear inter-layer cracks kinked into the core layer, propagated as opening-dominated intra-layer cracks and eventually branched as they attained high enough growth speeds causing core fragmentation.

Keywords: Debonding; Failure mode; Failure sequence; Impact; Sandwich material; Stress wave

1. Introduction

Layered materials and sandwich structures have diverse and technologically interesting applications in many areas of engineering. These include the increased use of composite laminates in aerospace and automotive engineering; the introduction of layered concrete pavements in civil engineering; the use of thin films and layered structures in micro-electronic components, and very recently, the introduction of sandwich structures in a variety of naval engineering applications (Hutchinson and Suo, 1992; Rajapakse, 1995; Valenti, 2001). In an entirely different length scale such materials and structures are also found in the natural layered rock structure of earth's crust. While failure characteristics of layered materials and sandwich structures subjected to static loading have been investigated extensively in the past years, their dynamic counterparts have remained elusive (Sun and Rechak, 1988; Cantwell and Morton, 1991;

* Corresponding author. Tel.: +1-626-395-4523; fax: +1-626-449-6359.
E-mail addresses: rosakis@aero.caltech.edu, rosakis@atlantis.caltech.edu (A.J. Rosakis).

0020-7683/02/$ - see front matter © 2002 Published by Elsevier Science Ltd.
PII: S0020-7683(02)00245-7

Abrate, 1994; Mines et al., 1999). Indeed, the presence of highly complex and transient dynamic failure modes in such materials and the inaccessibility of internal damage to real-time scruting have resulted in experimental studies limited to only the final impact damage characteristics of failure and to measurement of post-mortem residual strengths. To begin addressing the need for real-time observations of failure events, the work presented here focuses on the study of such events in model sandwich structures, and in particular, on the identification of their nature, chronological evolution and interaction.

To identify the evolution of failure modes for different loading regimes, it is convenient to first classify these modes based on the material constitutions of layered/reinforced structures. As shown schematically in Fig. 1, there are two major categories of failure observed in post-mortem studies. The first major failure category is decohesion (or cracking) between bonded layers at an interface. This is often referred to as delamination in composite laminates or interfacial debonding in thin films or sandwich structures. It is also called inter-layer failure. Generally, two distinct inter-layer failure modes are observed. The first one involves opening-dominated inter-layer cracking or "delamination buckling" (Vizzini and Lagace, 1987; Gioia and Ortiz, 1997; Kadomateas, 1999). The second one involves shear-dominated inter-layer cracks or "shear delaminations", and often occurs in layered materials subjected to out-of-plane impact (Wu and Springer, 1988; Choi et al., 1991; Lambros and Rosakis, 1997).

The second major category is referred to as intra-layer failure. There are three possible intra-layer failure modes depending on the material constitution. The first one is called intra-layer cracking or matrix cracking. This type of cracking often occurs inside the matrix of fiber-reinforced composites or within the soft core of sandwich structures (Lee and Daniel, 1990; Karandikar and Chou, 1992). It is also found in the form of tunneling cracks in thin film/substrate structures (Hutchinson and Suo, 1992; Shenoy et al., 2000). Another possible intra-layer failure is the failure of reinforcements such as fiber breakage and fiber kinking within a layer (Hahn and Williams, 1986; Oguni et al., 2000). The fifth possible intra-layer failure mode is interfacial debonding between the matrix material and the reinforcement (Ju, 1991) such as debonding

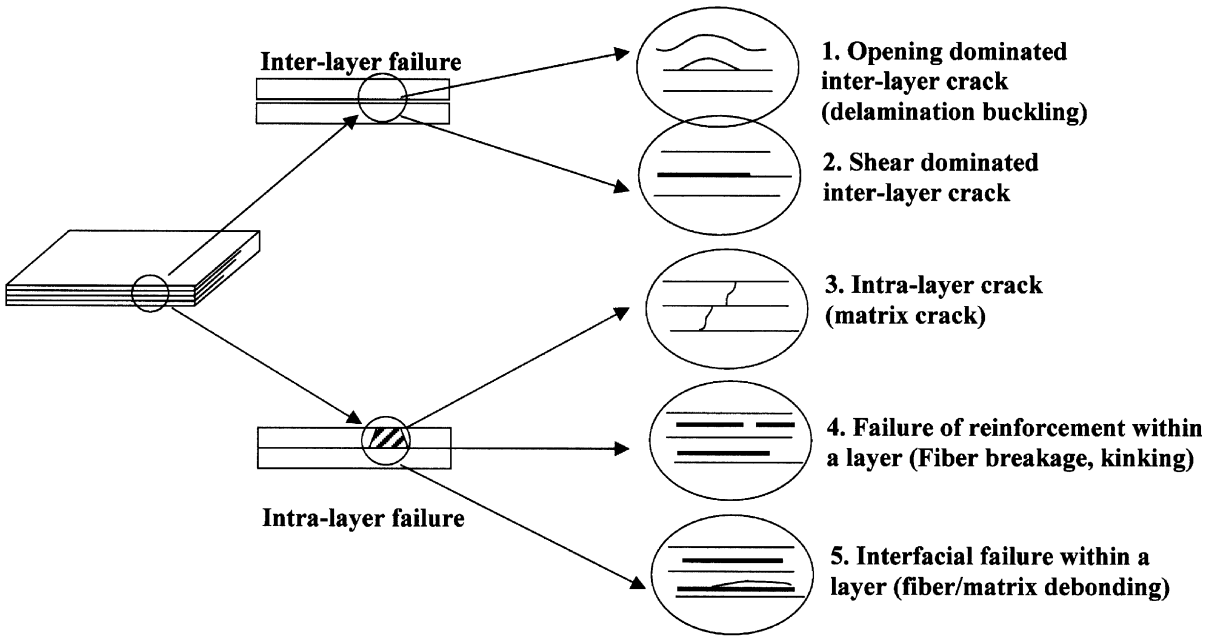

Fig. 1. Possible failure modes for layered materials based on material constitution.

between particle/fiber and matrix occurring within a constituent layer. As stated earlier, for most layered materials, the presence of such highly complicated dynamic failure modes and the inaccessibility of internal damage to direct observation explain the fact that only the final impact damage characteristics of such structures are usually discussed in the open literature. Indeed, the sequence, nature and interaction of such failure process were never properly clarified. Notable exception to this rule is the early studies of Takeda et al. (1982), who observed the evolution and sequence of matrix cracks and delamination failure in glass fiber composite laminates under ballistic impact. However, the equivalent situation involving low- or intermediate-speed impact loading has yet to be investigated.

In the recently emerging field of soft core, sandwich structures, the first studies of failure mechanisms have again concentrated on static loading conditions. The work of Li and Carlsson (1999) and his research group is pioneering in this aspect. In perhaps the first attempt to visualize impact failure in a real sandwich structure used in Naval applications, Semenski and Rosakis (1999) tested thin sections of such plate structures composed of PVC foam cores, sandwiched between E-glass faceplates. The sections were subjected to direct impact through a steel projectile traveling at a speed of 56 m/s. A pulsed laser was used to illuminate the specimens from the back side and a high-speed camera recorded the deformation and failure events. A sequence of photographs corresponding to this process is shown in Fig. 2 together with the post-mortem picture of the recorded specimen. As evident from the post-mortem picture, there are, at least, two types of failure present. Inter-layer failure demonstrates itself in the form of delamination between the face plates and the foam core at the vicinity of the impact site and free edges. On the opposite side, delamination

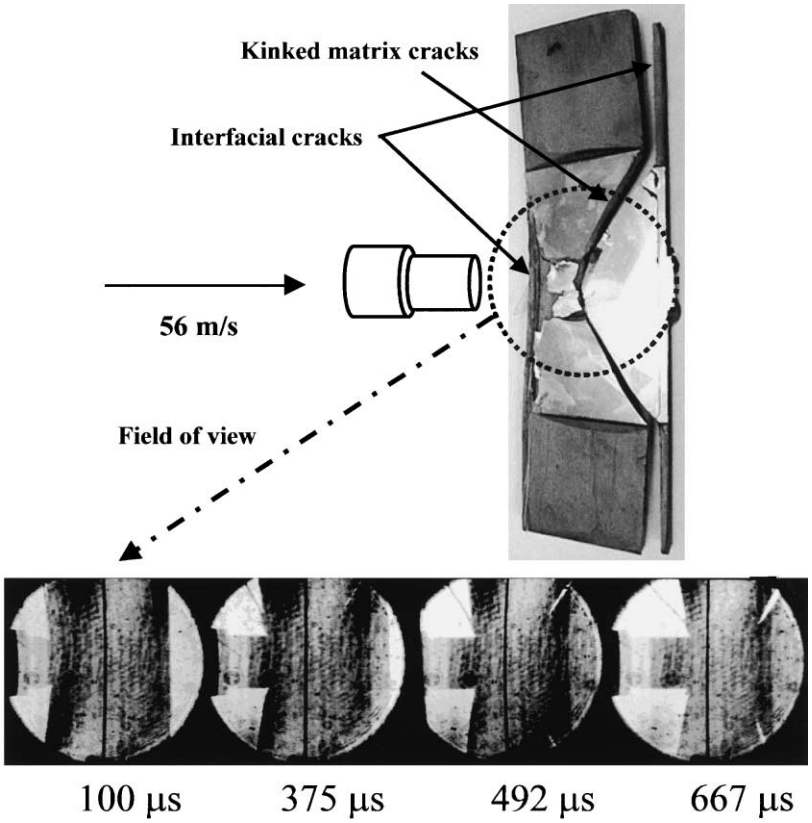

Fig. 2. A series of back-lit photos showing the dynamic failure process for a fiberglass face plates/PVC foam core sandwich structure.

is evident only on the top and on the bottom part of the specimen (away from the specimen center line). Intra-layer failure in the form of mode I, opening cracks in the soft core is also observed forming a highly symmetric pattern. Because the core is opaque, the high-speed pictures shown below are of limited use. What they show, however, is the emergence and propagation of the opening intra-layer (matrix) cracks inside the foam core. Indeed, these cracks seem to originate at the fiber glass/PVC interface opposite to the side of impact, and to symmetrically propagate towards the impact point. These cracks originate at the same location where the fiberglass/PVC delamination terminates. However, the time sequence and interaction between such inter-layer delaminations and the visible intra-layer, opening cracks in the core are not obvious. Indeed, the back-lit real-time photographs do not show any evidence of interfacial delamination within the time window of observation. As we will show later, this observation is misleading and is due to the fact that inter-layer fractures are typically shear-dominated. As such they do not allow for light to go through during the recording event because the shear crack faces remain in contact at the early stages of this process.

The inability of back-lit photography to visualize the failure process completely, motivates the use of partially transparent model sandwich systems which allow the use of full-field optical techniques capable of capturing the nucleation and growth of both opening and shear-dominated cracks and their transition from one mode to the other. For many complex engineering problems, model experiments may prove extremely useful as intermediate steps, which reveal the basic physics of the problem and provide relatively straightforward explanations of the failure patterns observed in post-mortem observations. A striking example of this approach was provided by Riley and Dally (1966), who designed a model metal/polymer layered system subjected to dynamic loading. Their model configuration was designed to simulate stress waves in layered structures. A similarly successful approach was adopted by Walter and Ravichandran (1997), who designed a model aluminum/PMMA/aluminum specimen to simulate and visualize the static debonding and matrix cracking process in ceramic matrix composites.

In our experiments, we also adopt the same idea and introduce an appropriate intermediate model configuration. In order to simulate the difficult three-dimensional problem of the out-of-plane impact of real sandwich structures and to simultaneously preserve the essence of the failure phenomena involved, we introduce a two-dimensional, plane stress specimen, which represents a cross-sectional cut of the layered material as illustrated in Fig. 3. For this type of model specimen, the failure process is easy to record,

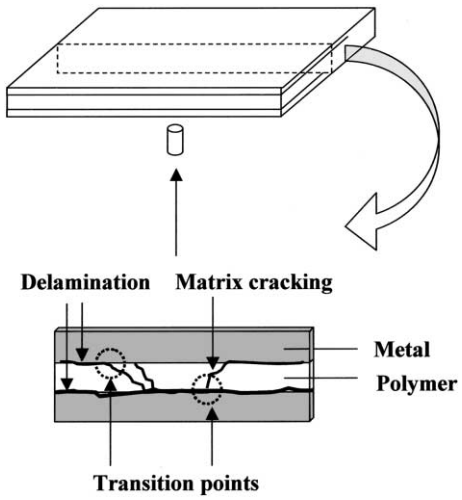

Fig. 3. Model layered specimens are idealized cross-sections of real structure subjected to out-of-plane impact.

visualize and analyze. It is noted that although the exact impact mechanics involved in two configurations is not identical (the real case is three-dimensional while the model specimen is closer to a plane stress state), the mechanisms of stress wave propagation and failure progression of the real and the model layered materials are quite analogous. In designing these model two-dimensional sandwich specimens, it is important to select model materials whose elastic mismatch is similar to that of materials used in real engineering applications (in our case PVC/composites). Selecting similar Dundurs' parameters (Hutchinson and Suo, 1992) may ensure similarity of the elasto-static response for the interfacial mechanics problem. Meanwhile, selecting model material combinations with similar ratios of wave speeds of two constitution materials to the real structure is perhaps the most important consideration in the dynamic case, where timing of events and stress intensity are governed by the constituent material wave speeds. Also, the ratio of inter-layer and intra-layer strengths (or fracture toughnesses) is important. These three issues provide sets of similarity rules to connect the real structures to our models tests.

As schematically shown in Fig. 3, matrix cracks and delamination are the two major impact failure modes in sandwich structures and composite laminates (Abrate, 1994). At some intersection points, matrix cracks and delamination are connected as also seen in the post-impact picture of Fig. 2. One frequently asked question in the literature is whether the matrix cracks lead to the delamination or the delamination happens first and subsequently kinks into the adjacent layer inducing the matrix crack. This is a typical problem of sequence and failure mode transition identification. In addition to these basic failure modes and the terminology discussed above, there is also further specialized classification common in the literature. Indeed, there are other types of matrix cracks called "bending matrix cracks", which are cracks that are straight and normal to the interface while matrix cracks inclined to the interface often carry the misnomer of "shear matrix cracks". So the nature of matrix cracks needs to be investigated.

Since the nature and origin of such failure mechanisms can only be theorized by post-mortem observations, the necessity of full-field real-time, high-speed measurements becomes obvious. To this effect, the objectives of the current work are to conduct systematic experimental studies of the time evolution and nature of different dynamic failure modes and to investigate their interactions. Through these model experiments, we try to identify the basic physical phenomena, and to provide guidance for theoretical models and much needed, real-time, validation of numerical codes. To make this comparison more meaningful, we choose model material combinations that have the ratios of wave speeds very close to those used in real sandwich structures. Their properties are discussed in the following section. The term 'low-speed impact' is used here to describe impact conditions such that the projectile speed is less than 30% of the speed of sound in air.

2. Experimental procedure

2.1. Materials and specimens

Two kinds of materials were used in the experiments described below. A 4340-carbon steel was employed to simulate the stiff and strong fiberglass faceplate of sandwich structures. The polymeric material, which was used to simulate the weak core layer, such as the PVC foam core or balsa wood in sandwich structures or the 90° plies in cross-ply laminates, is Homalite-100. Some physical properties of these model materials are listed in Table 1. The adhesive used to bond the metal/polymer interface is Weldon-10. The detailed properties of this adhesive and the effect of interfacial strength variation on dynamic failure mode selection are reported in Part II of this investigation (Xu and Rosakis, 2002a).

The shear wave speed is an important parameter in this investigation. The shear wave speed ratio for the core and faceplate is 3.2 for typical E-glass/PVC sandwich structures of the type that have recently been used in construction of full-scale composite ships (Valenti, 2001) (e.g., the Swedish "Visby" class corvettes).

Table 1
Material properties used in model experiments

Property	Homalite 100		Steel 4340
	Static	Dynamic[a]	Static
Young's modulus E (GPA)	3.9	5.3	208
Poisson's ratio v	0.35	0.35	0.3
Dilatational wave speed c_l (m/s) (plane stress)	1890	2119	5500
Shear wave speed c_s (m/s)	1080	1208	3320
Rayleigh wave speed c_R (m/s)	1010	1110	2950
Density ρ (kg/m^3)	1230	1230	7830

[a] Dynamic properties correspond to an average equivalent strain rate of 10^3/s.

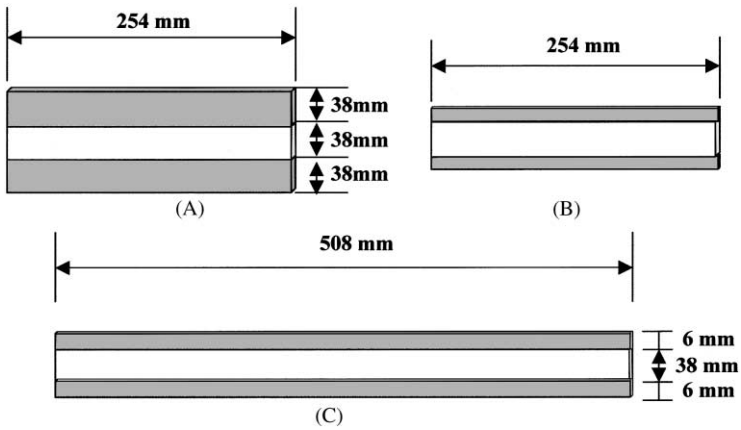

Fig. 4. Model specimens simulating sandwich structures (shaded layers—metals; transparent layers—polymers).

Details on the complete set of physical and constitutive properties for E-glass composite materials have recently been discussed by Oguni et al. (2000). For comparison, the same shear wave speed ratio, for the idealized steel/Homalite model sandwiches, is about 2.7 based on the data from Table 1. Although the absolute values of these constituent properties are very different in the "idealized" versus the "real" solids, the idealized material combinations have been chosen in such a way as to have a shear wave speed ratio that is very similar to its real sandwich counterparts.

As shown in Fig. 4, three different types of model sandwich specimen geometries were designed and tested. Type A specimens have equal layer widths and involve two different materials. They contain two metal layers with one polymer layer sandwiched between them. Type B specimens involve two thin metal layers (faceplates) and one polymer layer. This type of specimens is quite similar in geometry (ratio of core to face plate thickness) to realistic sandwich plates used in engineering applications. The only difference between type C and type B specimens is their lengths. Type C specimens are twice as long as type B specimens. The purpose of type C specimens is to explore the impact failure patterns with least edge effect present in the time scale of the failure process. All three types of specimens have the same out-of-plane thickness of 6.35 mm (0.25 in.).

2.2. Experimental setup

The majority of experiments in this investigation were performed using dynamic photoelasticity. This classical method has recently found a lot of new applications such as study of the dynamic fracture pro-

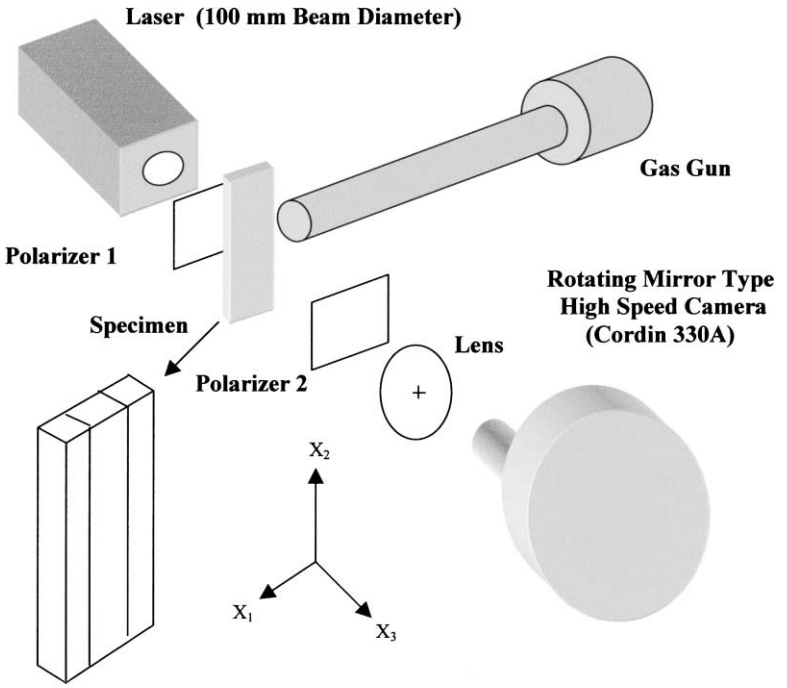

Fig. 5. Schematic of the dynamic photoelasticity setup.

cesses in functionally gradient materials described by Parameswaran and Shukla (1998). The coherent gradient sensing method (Rosakis et al., 1998) was also used in a small number of cases. A schematic of the dynamic photoelasticity setup used here is given in Fig. 5. Two circular polarizer sheets were placed on either side of the specimen. An Innova Sabre argon-ion pulsed laser was used as the light source. The coherent, monochromatic, plane polarized light output was collimated to a circular beam of 100 mm in diameter. The laser beam was transmitted through the specimen and the resulting fringe pattern was recorded by the high-speed camera. A Cordin model 330 A rotating-mirror type high-speed film camera was used to record the images. During the impact test, a projectile was fired by the gas gun and impacted the specimen center. The generation of isochromatic fringe patterns is governed by the stress-optic law. For the case of monochromatic light, the condition for the formation of fringes can be expressed as (Dally, 1979):

$$\hat{\sigma}_1 - \hat{\sigma}_2 = \frac{N f_\sigma}{h}$$

where $\hat{\sigma}_1 - \hat{\sigma}_2$ is the principal stress difference of the thickness averaged stress tensor. f_σ is the material fringe value, N is the isochromatic fringe order and h is the specimen thickness. The isochromatic fringe patterns observed are proportional to contours of constant maximum in-plane shear stress, $\hat{\tau}_{\max} = (\hat{\sigma}_1 - \hat{\sigma}_2)/2$.

3. Results and discussion

3.1. Failure process in type A specimens (with equal layer widths and a short length)

The diameter of the laser beam used in this investigation was 100 mm; however, the maximum length of the zone that had to be investigated was 254 mm long. In order to observe all possible dynamic failure

modes present in each case, the field of view had to be moved from one location to another for each specimen configuration under the same impact condition. Fig. 6 presents a series of photoelastic images of the Homalite core layer of a type A specimen. In all these experiments, the projectile impacted the center of the bottom metal layer. The dark circular spot at the upper right corner is a scaling mark (diameter 6.35 mm) bonded on the specimen. The thin horizontal dark line, seen around the center of every image, is the streak line of the camera. This line provides a stationary reference when the whole specimen moves during the impact process. At first, the field of view was centered on the middle of the specimen because it was close to the impact position and failure was expected to initiate from this zone. As shown in Fig. 6(b), about 158 μs after impact, two inter-layer cracks at the lower interface entered the field of view (from the right and left respectively) and propagated towards the specimen center. Before that time, there was no visible damage

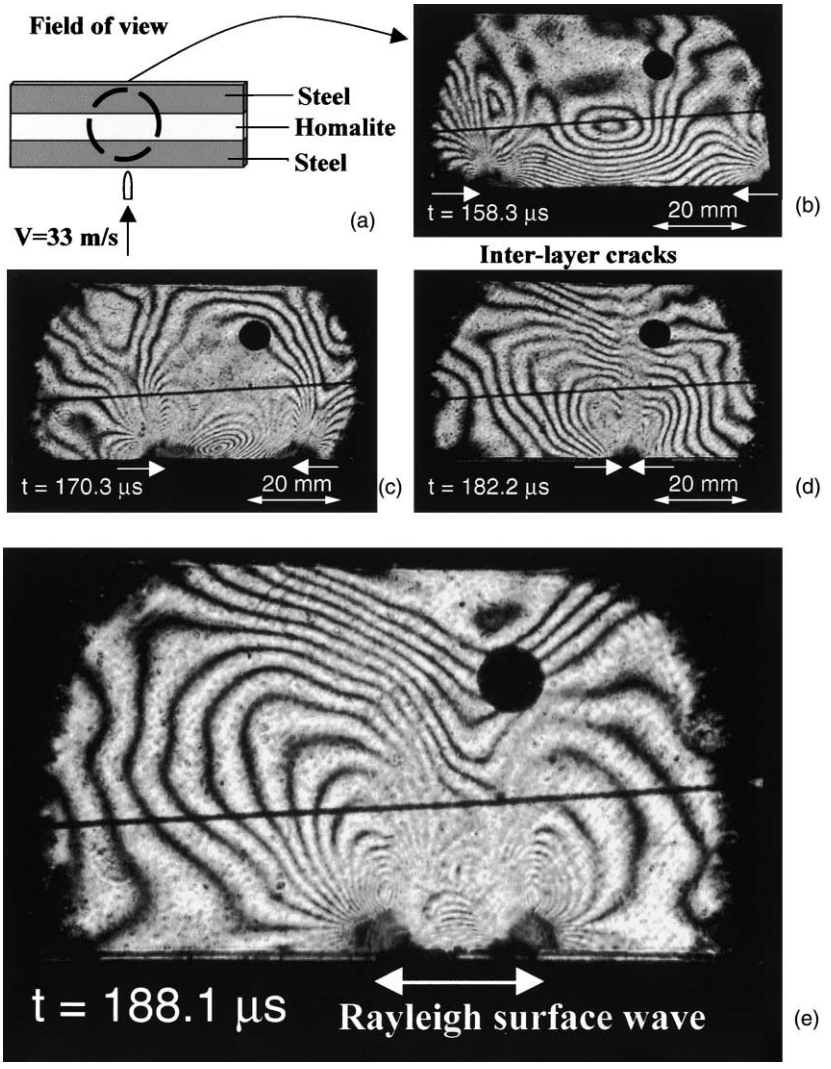

Fig. 6. Early stages of the failure process of a three-layer specimen with equal layer widths. The central field of view reveals the early occurrence of shear-dominated delamination at the lower interface. At later times (e), the debonding becomes clearly visible at the lower interface.

within the field of view. Later on (around 182 μs), the two inter-layer cracks, identified by the moving concentration of fringes at their tips, are seen to meet each other in Fig. 6(d). Similar to shear-dominated interfacial cracks in bimaterials (Lambros and Rosakis, 1995; Singh and Shukla, 1996), those inter-layer cracks are also shear-dominated. Because the Homalite and steel layers are still in contact up to that time, no visual evidence of decohesion is apparent in the images, although these cracks have already broken the interface in a combination of compression and shear. After these two inter-layer cracks meet at the center, a bright gap between the Homalite and steel layers can be seen to appear in Fig. 6(e). Along this clearly opened interface and on the Homalite side, two Rayleigh surface waves are now seen to propagate, originating from the center and moving outwards, the specimen edges. The crack speed history for one of the two lower inter-layer cracks is plotted in Fig. 7. The dynamic shear wave speed of Homalite-100 (see Table 1) is also shown as a horizontal dashed line. This value has been obtained experimentally by the procedure outlined by Xu and Rosakis (2002b).

Within the resolution of our measurement, the interfacial (inter-layer) crack tip speed remains very close to the shear wave speed of the core material (Homalite-100) and exhibits temporary subsonic and intersonic fluctuations. This is a phenomenon very similar to the one reported by Lambros and Rosakis (1995), who looked at the dynamic fracture behavior of metal/polymer bimaterial interfaces subjected to asymmetric impact loading. Indeed, for moderate impact speeds the interfacial cracks were seen to accelerate unstably to the shear wave speed of the polymer and to fluctuate above that value before more energy was provided to the system at which instant they became clearly intersonic. The dependence of this behavior on impact speed and bond strength was recently analyzed by Needleman and Rosakis (1999) with very similar conclusions. In the present case, the inter-layer crack speeds are too close to the shear wave speed of Homalite-100 to exhibit the clear shock wave structure characteristics of intersonic fracture. However, as the impact speed is increased, this structure will become clearly visible in the high-speed impact experiments to be presented in Part II of this work (Xu and Rosakis, 2002a).

Perhaps the most interesting conclusion deriving from the sequence shown in Fig. 6 is the fact that delamination did not initiate in the interface directly above the impact point but did so outside our central field of view at two symmetric, off-axis, locations along the lower interface. In order to discover the location of crack nucleation, we must move our field of view off the specimen center to investigate the origins of these inter-layer cracks. To achieve this we first center our field of view to the middle between the specimen edge and the center, as shown in Fig. 8(a). The loading condition and geometry are intentionally kept identical. About 129 μs after impact, an inter-layer crack at the lower interface entered the field of view from the left and propagated towards the specimen center. This crack eventually met with its symmetric counterpart at the specimen center as shown in Fig. 6. As explained earlier, the interface first broke in shear

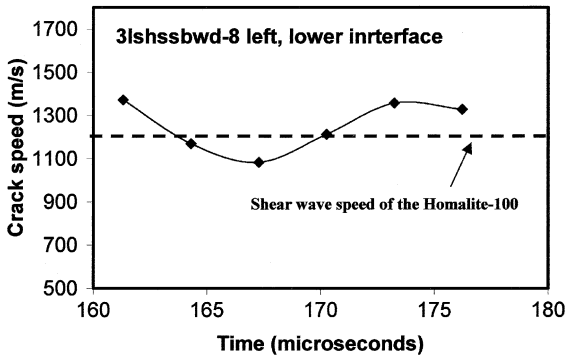

Fig. 7. Crack speed history of one of the two inter-layer cracks at the lower interface.

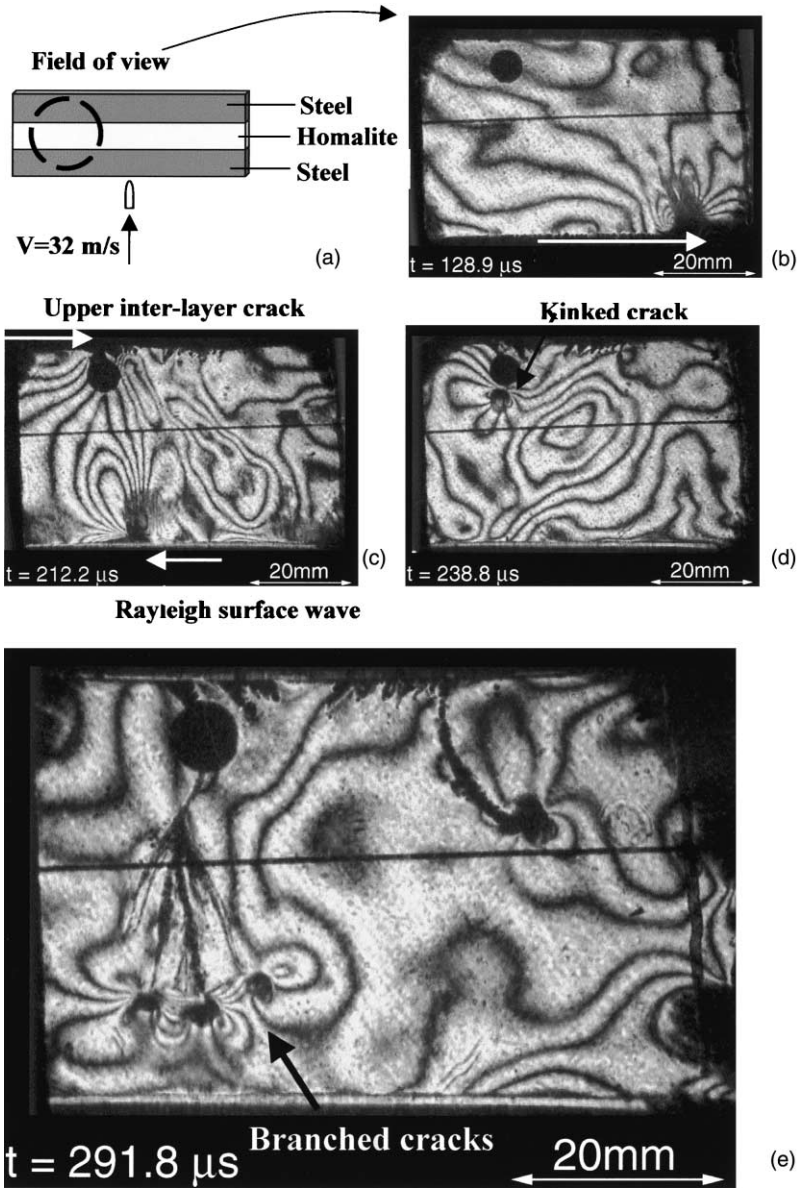

Fig. 8. Dynamic failure modes and sequence in a layered specimen from a different field of view. Following interfacial delamination at the lower then the upper interfaces, cracks kink into the core layer to form intra-layer damage.

and afterwards separated to form a visible gap. A Rayleigh surface wave was then formed and propagated along the resulting free surface. The Rayleigh wave started from the specimen center and propagated towards the specimen edge as shown in Fig. 8(c). Meanwhile, as also shown in Fig. 8(c), another inter-layer crack appeared at the upper interface and also propagated towards the center. At a location close to the circular mark (dark dot), the upper inter-layer crack kinked into the Homalite core layer thus forming an intra-layer crack (matrix crack) as shown in Fig. 8(d). After a short period of acceleration, the kinked crack branched into a fan of cracks shown in Fig. 8(e). Crack branching as reported by previous researchers often

initiates when a crack in a homogeneous solid reaches high fractions of the shear wave speed (Ravi-Chandar and Knauss, 1984), for example, 30–40% shear wave speed of Homalite-100. Based on this observation, we can conclude that the kinked intra-layer cracks (matrix cracks) occur after the formation of both (lower and upper) inter-layer cracks (delamination cracks). These kinked cracks are of the purely mode I type (opening mode) and are typical of all cracks in any homogeneous, isotropic solids. This phenomenon is indeed consistent with our early discussion of failure in real fiberglass/PVC sandwich structures presented in the introduction (see Fig. 2). The photoelastic investigation merely confirms our earlier suspicion that shear-dominated delamination occurs first. It is only later followed by cracks kinking into the core layer from the side opposite to the impact point and moving towards the impact location. We suspect that this is also what happens in the fiber-reinforced composite laminates studied by Sun and Rechak (1988). Here again the cracks kinking to the central 90° layer are opening-dominated rather than shear-dominated, although they are often referred to "shear matrix cracks" in the literature. Because fiber-reinforced composite materials show transversely isotropic mechanical properties (Vinson and Sierakowski, 1986), mode I opening cracks rather than mode II shear cracks occur in the 90° central layer.

In order to conclusively identify the origins of the upper and lower inter-layer cracks, the field of view was once more moved to the specimen edge as shown in Fig. 9(a). After impact at the specimen center, the

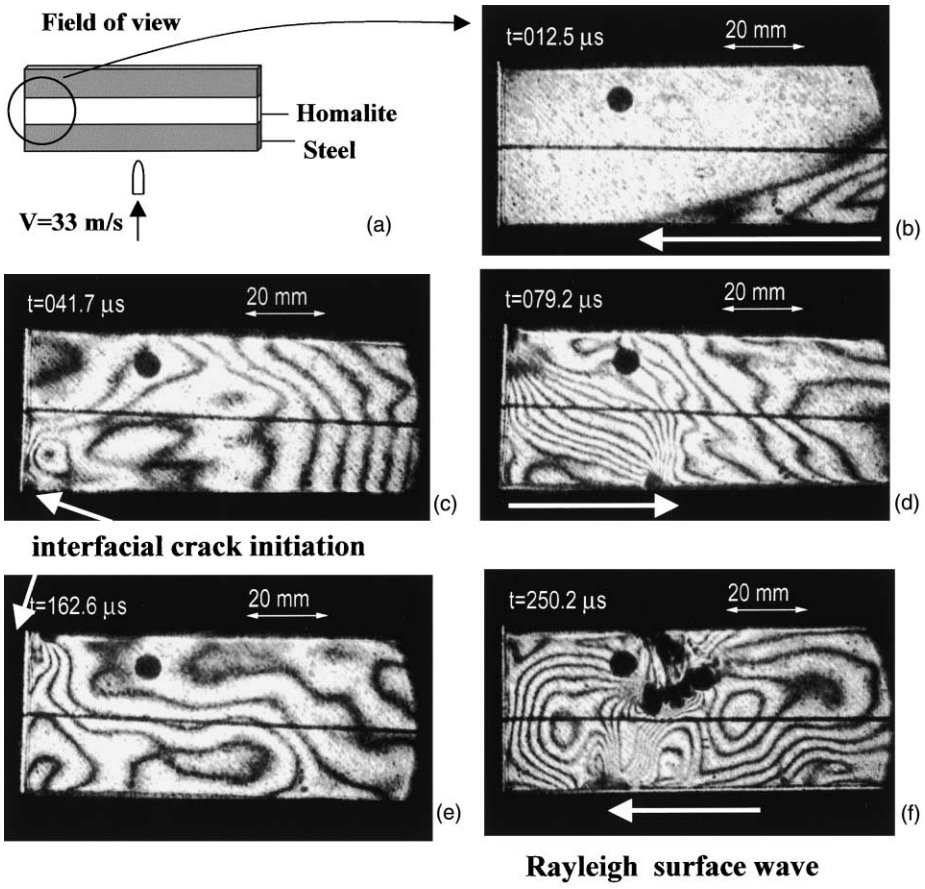

Fig. 9. An edge view of damage evolution. Inter-layer delaminations are shown to form at the intersection of, first lower, and then upper interfaces with the specimen edge. A fan of kinked intra-layer cracks branches into the core layer from the upper interface.

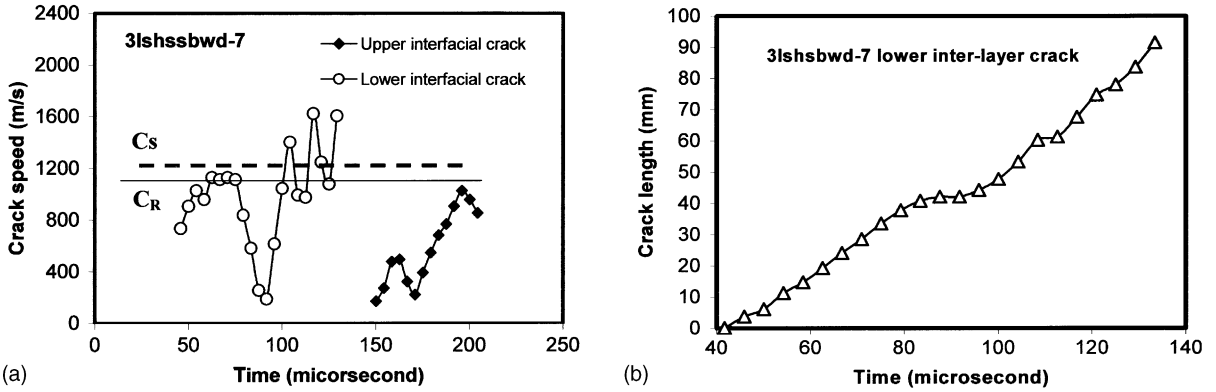

Fig. 10. Crack speed history (a) of two inter-layer cracks and crack length (b) history of the lower inter-layer crack. C_s and C_R are the shear wave and Rayleigh wave speeds of Homalite-100.

stress waves in the bottom steel layer propagated towards the edge creating a visible head wave structure on the lower wave speed polymer side (see Fig. 9(b)). Right after the stress wave reached the free edge, due to the existence of a stress singularity at the bimaterial corner (Williams, 1952), an inter-layer crack initiated at the lower interface as seen in Fig. 9(c). This crack propagated towards the specimen center. After around 160 μs, another inter-layer crack initiated at the upper interface also moving towards the center. This upper inter-layer crack soon kinked into the core layer and branched into a fan of multiple mode I intra-layer cracks. This process is very consistent with the result of Fig. 8 demonstrating the repeatability of this phenomenon.

The speed history of two inter-layer crack tips is presented in Fig. 10(a). It is noticed that the inter-layer crack at the lower interface can reach intersonic speeds but the inter-layer crack at the upper interface is a purely subsonic crack. It is interesting to note that the crack speed of the lower inter-layer crack reached the Rayleigh wave speed of Homalite-100 within 20 μs after the crack initiation. However, the crack speed suddenly dropped to a very low value (close to zero) around 90 μs after impact. Then, the crack speed again increased dramatically and fluctuated to intersonic and subsonic levels about the shear wave speed of Homalite-100. The maximum recorded crack tip speed was close to $\sqrt{2}C_s^H$, where C_s^H is the shear wave speed of the Homalite core layer. The crack speed history is obtained by numerically differentiating the crack length history, shown in Fig. 10(b). Fig. 11 shows the global trends of the lower inter-layer crack tip speed plotted as a function of position from the specimen free edge. Results from all three identical specimens subjected to the same impact conditions, discussed earlier, are collectively displayed in this figure. In these experiments, the field of view varied from the specimen edge all the way to the specimen center. The crack tip speed seems to increase as the distance from the specimen edge increases; it then decelerates at about 30 mm from the edge and then drastically accelerates to intersonic levels as the specimen centerline is approached, never exceeding $\sqrt{2}C_s^H$. The significance of the special speed $\sqrt{2}C_s^H$ is discussed by Lambros and Rosakis (1995).

Based on experimental observations from three different fields of view, the major dynamic failure modes and sequence in model three-layer materials can be summarized in Fig. 12. After the stress wave reaches the free edges, two shear-dominated inter-layer cracks initiate and propagate towards the specimen center. These shear cracks separate the whole lower interface and a Rayleigh surface wave forms on the separated free surface. This wave splits into two and travels from the specimen center to the edges. At a later stage, inter-layer cracks also originate from the upper interface at the free edge and travel towards the specimen center. However, these upper inter-layer cracks soon kink into the core layer to form opening-dominated intra-layer cracks. Under certain circumstances (e.g., if the core material is very brittle), such kinked cracks

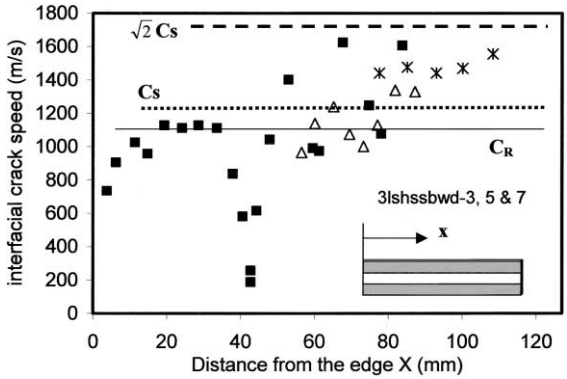

Fig. 11. Crack speed distribution as a function of distance from the specimen edge. Results from three experiments under the same conditions are shown.

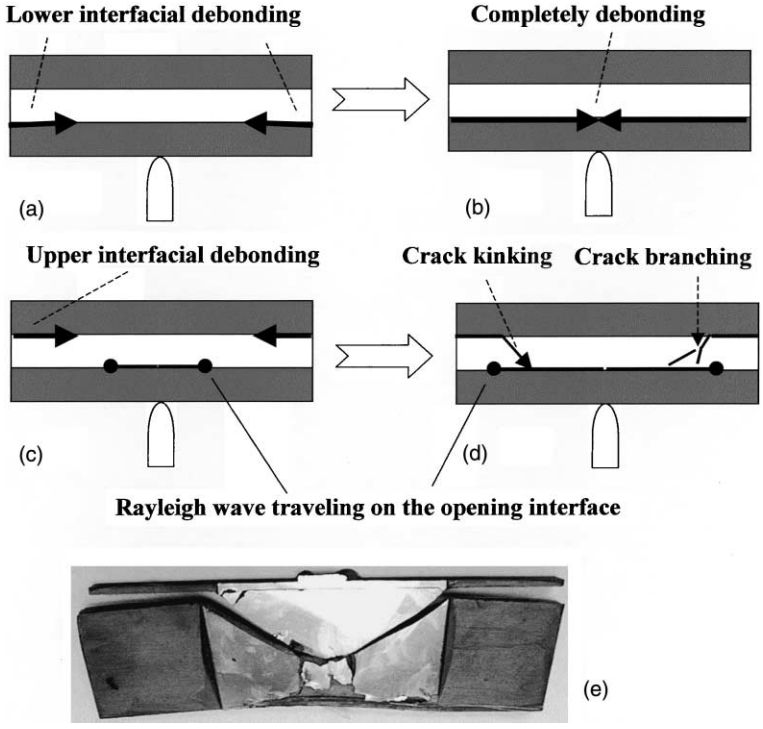

Fig. 12. Conceptual summary of typical failure modes and sequence in a short three-layer specimen with equal layer widths; (e) is a comparison with a post-impact picture of a real sandwich specimen.

may also branch into a fan of multiple branches fragmenting the core. The model experiments described here seem to capture the basic nature of the post-mortem impact failure modes observed in real sandwich structures. Indeed, the kinked matrix crack of the core layer of the glass fiber/foam core sandwich shown in Fig. 12(e) seems to follow the same initiation and propagation process as the kinked intra-layer crack in the model three-layer specimens schematically shown in Fig. 12(d). Actually, the so-termed "shear matrix

cracks'' or ''shear core cracks'' discussed in post-mortem studies of failure in composite or sandwich structures (Abrate, 1994; Wen et al., 1998; Karbhari and Rydin, 1999) are instead opening-dominated, as clearly seen by the optical patterns of Figs. 8(e) and 9(f) and, as such, they are inappropriately named.

3.2. Failure process in type B specimens (short sandwich-style specimens)

Fig. 13 shows a photoelasticity sequence of photographs corresponding to a type B specimen with thin metal layers. This type of specimen is quite similar to a real sandwich structure in terms of the thickness ratio of the faceplate to core. The field of view on the specimen edge is shown in Fig. 13(a). The failure process in this type of specimens is quite similar to the process observed in type A specimens, summarized in the previous section. The failure mode occurring first is still the inter-layer crack at the lower interface. However, when the impact speed is lower (here is 10 m/s compared to 33 m/s in the previous case), this inter-layer crack initiates very late as shown in Fig. 13(c). The crack tip speed history of the inter-layer

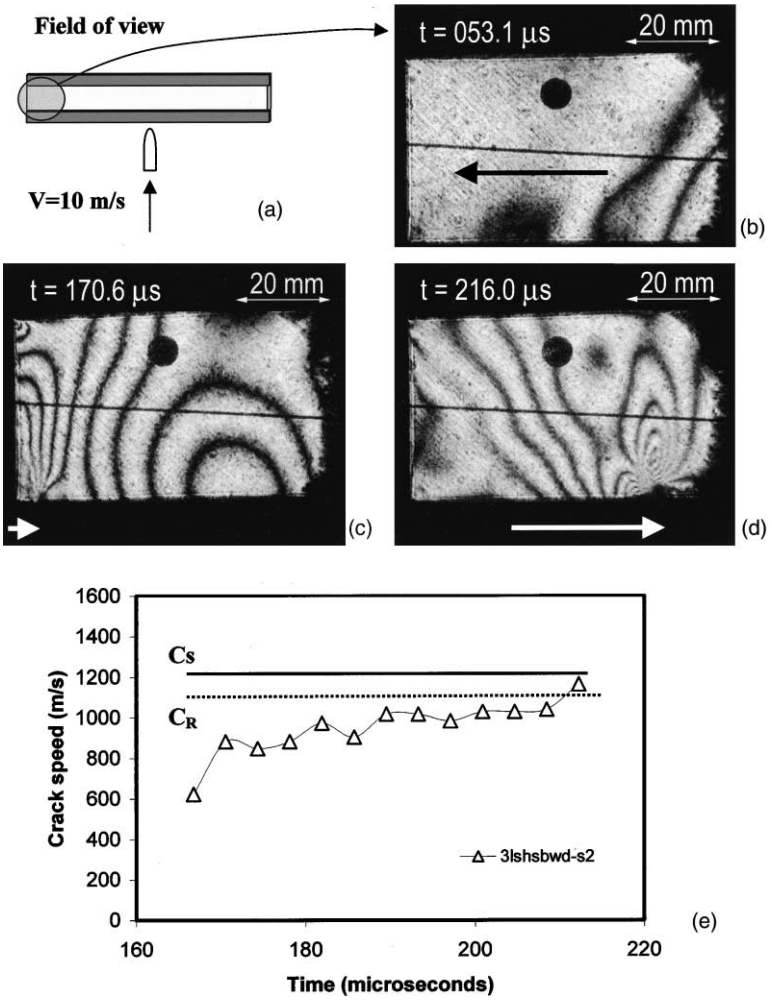

Fig. 13. Inter-layer crack initiation and propagation at the lower interface of a model sandwich-style specimen (type B specimens).

crack is shown in Fig. 13(e) as a function of time. The crack initiates at a high subsonic speed at around 600 m/s and accelerates monotonically to a value close to the Rayleigh wave speed of Homalite-100. In Part II of this investigation (Xu and Rosakis, 2002a), we briefly study the effects of impact speed and interfacial bond strength on the speed of such inter-layer cracks.

3.3. Failure process in type C specimens (long sandwich-style specimens)

In types A and B specimens, inter-layer cracks always initiated from the specimen free edges due to the stress concentration at such locations. In order to study the impact damage modes and failure sequence in either very large structures or ones that are clamped along the edges, our model specimens featured long specimens. These specimens were long enough such that any damage from the edges, such as inter-layer

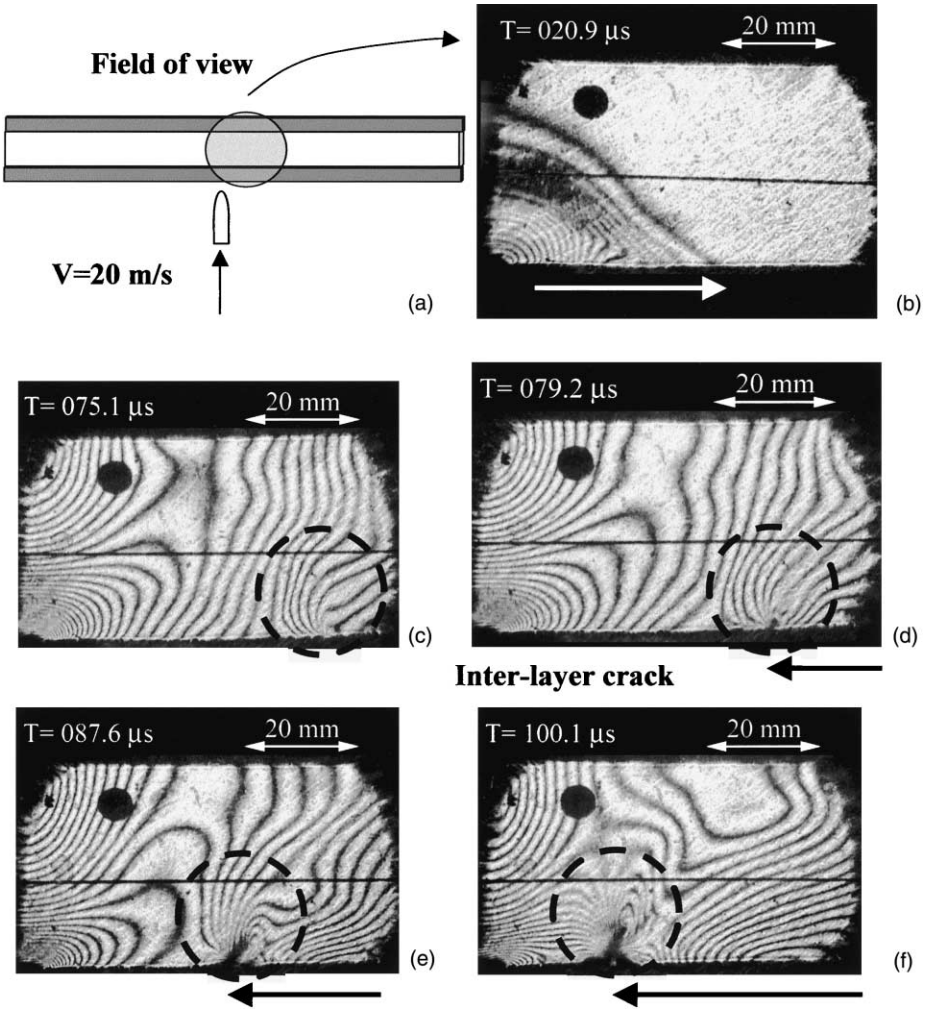

Fig. 14. Nucleation of an intersonic inter-layer crack at the vicinity of the impact area. The specimen (type C specimens) is long enough to eliminate the edge interference.

cracks induced by the edge effect, arrived in the area of observation long after the local damage sequence had been completed near the impact point. To study this effect, we tested long sandwich-style specimens of type C (see Fig. 14). As shown in Fig. 14(d), at 79 μs after impact, an inter-layer crack tip is seen at the lower interface (fringe concentration within the dashed circle). This crack is similar in nature to our previously observed inter-layer fractures but has not originated at the specimen free edge, which for type C specimens is far away from our field of view. Indeed, if this crack originated from the specimen free edge, it would take at least 150 μs to enter the field of view. Closer scrutiny reveals that this crack originates from a much closer location to the impact point. This location is marked here by the circle in Fig. 14(c) within which a concentration of photoelastic fringes points to the concentration of shear stresses that is responsible for its nucleation. Indeed the crack nucleates at a location where the inter-layer shear stress reaches a local maximum, whose value equals the shear strength of the bond. To rationalize this, one should consider the symmetry of our impact configuration and recall the strong wave speed mismatch between the lower faceplate and the core material. The shear stress component σ_{12} at the specimen centerline will always vanish because of this symmetry but is expected to anti-symmetrically increase away from the centerline as compressive waves begin to spread along the steel faceplate. A simple wave diagram showing the creation of intense shearing along the lower interface because of the wave speed mismatch is shown in Fig. 15. The diagram clearly shows that as points P_1 and P_2 move symmetrically away from the centerline, they load it in a combination of compression and shear. This combination is what is needed to generate the intersonic shear-dominated inter-layer cracks that are consistently observed throughout this work and are similar to

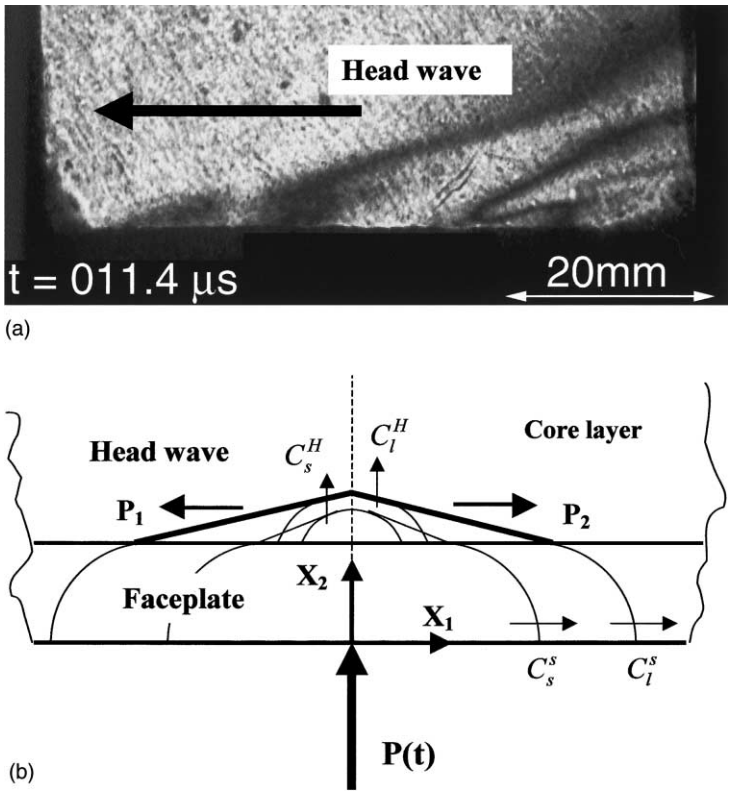

Fig. 15. Wave diagram (b) and picture demonstrating the mechanism of compression/shear loading of the lower interface of a sandwich structure subjected an impact loading at the center of lower faceplate.

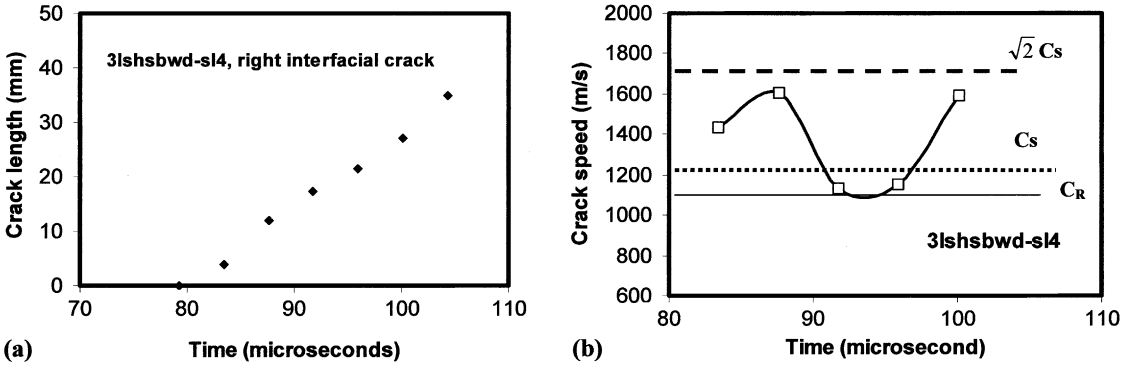

Fig. 16. Crack length history (a) and crack speed history (b) of the lower interfacial crack nucleated at the central part of a long model sandwich specimen.

the original bimaterial studies of Lambros and Rosakis (1995), subsequently analyzed by Needleman and Rosakis (1999). If the impact speed is high enough, or the specimen is long enough, there would be a time when the shear stresses at P_1 and P_2 will reach a critical level, high enough to nucleate two inter-layer cracks

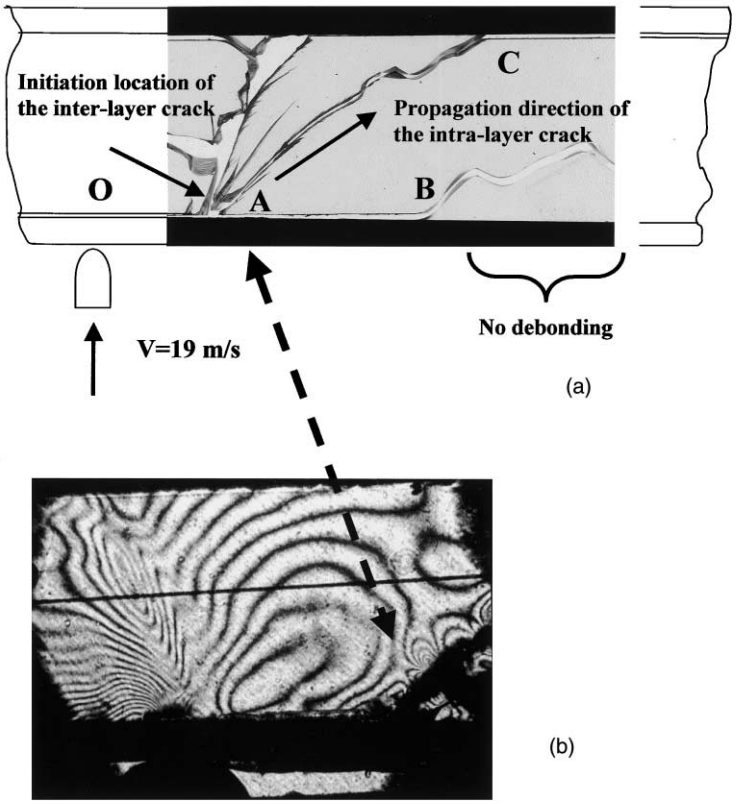

Fig. 17. Local view of the post-mortem damage in a long sandwich-style specimen (a) and high-speed snap shot capturing the formation of intra-layer cracks (b).

before either P_1 or P_2 reach the specimen edges. If on the other hand, the impact speed (and thus the magnitude of the induced interfacial shear) is not very high, then shear delamination would not occur until P_1 and P_2 reach the edges where the shear stresses will be amplified by the edge singularity to cause delamination. It is this later case which dominated the failure behavior in the "short" type A and B specimens. The hypothesis presented above is indeed consistent with the previous finite element analyses of composite laminates subjected to out-of-plane impact (Sun and Rechak, 1988; Choi et al., 1991) where two clear peak values (same magnitude) of the interlaminar shear stress were shown to symmetrically move away from the impact site (i.e., the specimen center, where the interlaminar shear stress is zero according to geometrical symmetry). Of course, the amplitude of these peaks depends strongly on the impact speed and on the stress wave mismatch between faceplates and core materials. As a result of these observations, the scenario that seems to be emerging is as follows: shear-dominated cracks are generated at two points to the right and left of the center line and move towards the impact point. A series of photographs confirming the existence of an inter-layer crack coming from the right-hand side of the impact point is shown in Fig. 14. Indeed Fig. 14(c) corresponds to the nucleation of this crack while Fig. 14(d)–(f) confirm its high-speed motion towards the impact site. As this inter-layer crack and its symmetric companion from the left meet above the impact point, they create a central shear delamination between the core and the bottom faceplate. The speed of this crack is very high as evident from the shear shock wave that appears as a dark inclined line radiating from its moving tip (Fig. 14(e) and (f)). This is confirmed by the crack length and speed histories shown in Fig. 16.

Fig. 17 corresponds to another impact experiment which featured the same load condition as shown in Fig. 14. The end point of the central delamination described above is denoted by A. Fig. 18 shows the

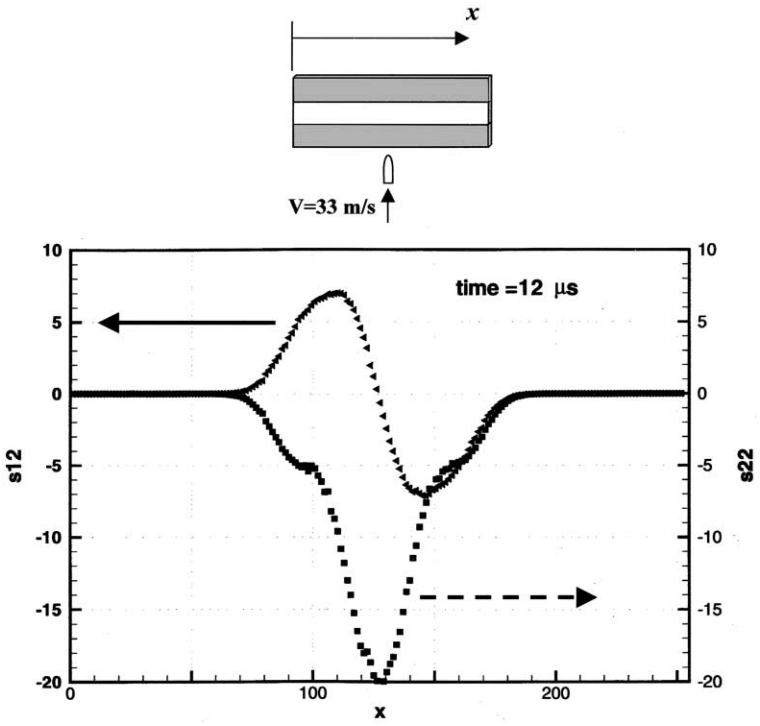

Fig. 18. Variations of inter-layer normal and shear stress along the interface of a long sandwich-style specimen after impact (Yu et al., 2001).

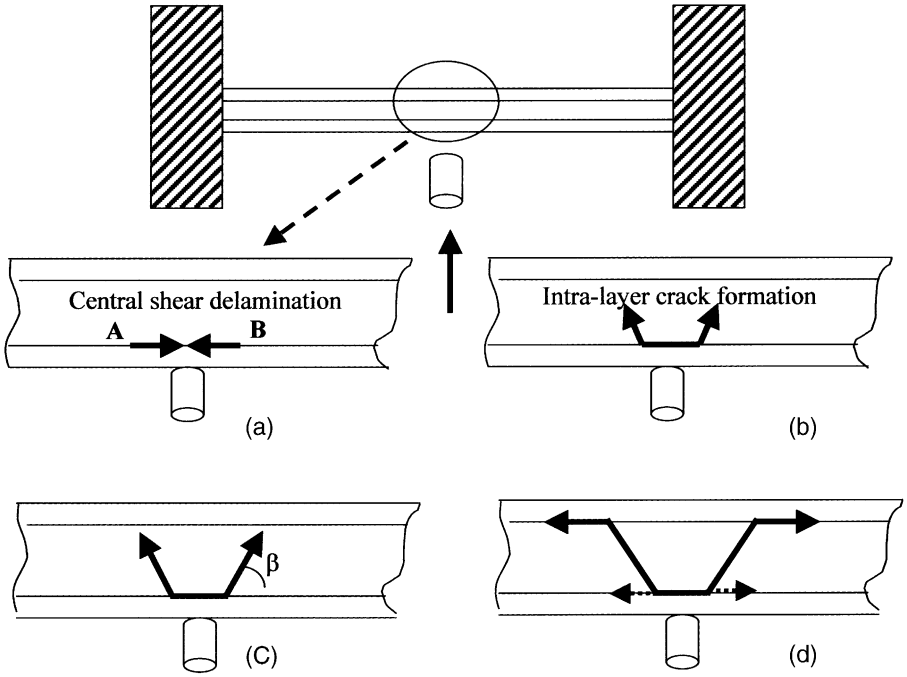

Fig. 19. Failure sequence observed in long sandwich-style specimens with minimal edge effects.

variations of the inter-layer shear and normal stress at the interface of this model sandwich specimen simulated by Yu et al. (2001). As shown in Fig. 18, the inter-layer normal stresses near the impact point are compressive while the inter-layer shear stresses exhibit two clear peak values (same magnitude) moving symmetrically away from the centerline. Point A in Fig. 17 is corresponding to the old location of the maximum inter-layer shear stress. This point can now acts as a stress concentration from which further damage (to the core as well as to the rest of the interface) will subsequently evolve. Indeed as seen in Fig. 17, intra-layer cracks now are generated and propagated into the core (along AC), also accompanied by a new inter-layer debond (along AB) also originating at point A. The high-speed snapshot that appears in the same photograph confirms this scenario. Fig. 19 summarizes the proposed failure evolution sequence for the long sandwich-style specimens described above. One point that should be made clear here is that following the formation of the central (shear) delamination, the choice of the inclination angle β and the possibility of further delamination along the bottom interface depend on the impact speed and on the relative values of the matrix material and interfacial bond strengths. The same is true for the exact locations of points A and B. However, we expect that if impact speeds are high enough to promote this localized failure mode, the general features described here will continue appearing even as the projectile speed increases further. An extension of the present work concentrating on the effect of bond strengths and impact speeds on dynamic failure is presented in Part II of this investigation. For the initiation of intra-layer cracks (matrix cracks), previous researchers theorized that such cracks initiated from the center of the weak layer and propagated toward adjacent interfaces to lead to inter-layer cracks or delaminations (Choi et al., 1991; Geubelle and Baylor, 1998). However, no real-time experimental evidence was ever observed to support such a scenario. Here, we clearly show that the intra-layer cracks always initiate at the interfaces immediately following the shear-dominated delamination fracture, which kinks into the core layer resulting in intra-layer core cracking.

4. Conclusions

In all cases described in this paper, inter-layer crack growth (delamination) is the dominant dynamic failure mode for layered materials and sandwich structures. These cracks appear to be shear-dominated and proceed with intersonic speeds. Intra-layer cracking always occurs soon after some amount of inter-layer delamination has already happened and proceeds through the spreading and branching of local mode I cracks into the core layer. Intra-layer or core cracking often initiates at the interface as a result of inter-layer crack kinking into the core. If the speed of the kinked intra-layer crack reaches a critical value, multiple crack branching may also occur inside the core layer. If free edge effects at the bimaterial corners are eliminated, the failure sequence is slightly modified. Specifically, the inter-layer cracks initiate from positions where the inter-layer shear stress reaches a local maximum equal to the shear strength of the bond. These cracks create a local shear driven delamination directly above the point of impact. Intra-layer cracks following this process also kink from these positions into the sandwich core.

Acknowledgements

The authors gratefully acknowledge the support of the Office of Naval Research (Dr. Y.D.S. Rajapakse, Project Monitor) through a grant (#N00014-95-1-0453) to Caltech. The assistance of Dr. Demir Coker and Dr. David Owen is greatly appreciated.

References

Abrate, S., 1994. Impact on laminated composites: recent advances. Appl. Mech. Rev. 47, 517–544.

Cantwell, W.J., Morton, J., 1991. The impact resistance of composite materials—a review. Composites 22, 347–362.

Choi, H.Y., Wu, H.T., Chang, F.-K., 1991. A new approach toward understanding damage mechanisms and mechanics of laminated composites due to low-velocity impact: part II—analysis. J. Compos. Mater. 25, 1012–1038.

Dally, J.W., 1979. Dynamic photoelastic studies of fracture. Exp. Mech. 19, 349–361.

Geubelle, P.H., Baylor, J.S., 1998. Impact-induced delamination of composites: a 2D simulation. Composites Part B 29B, 589–602.

Gioia, G., Ortiz, M., 1997. Delamination of compressed thin films. Adv. Appl. Mech. 33, 119–192.

Hahn, H.T., Williams, J.G., 1986. Compression failure mechanisms in unidirectional composites. In: Whitney, J.M. (Ed.), Composite Materials: Testing and Design (7th Conference), ASTM STP 893, American Society for Testing and Materials, pp. 115–139.

Hutchinson, J.W., Suo, Z., 1992. Mixed mode cracking in layered materials. Adv. Appl. Mech. 29, 63–191.

Ju, J.W., 1991. A micromechanical damage model for uniaxially reinforced composites weakened by interfacial arc microcracks. J. Appl. Mech. 58, 923–930.

Kadomateas, G.A., 1999. Post-buckling and growth behavior of face-sheet delaminations in sandwich composites. In: Rajapakse, Y.D.S., Kadomateas, G.A. (Eds.), Thick Composites for Load Bearing Structures, AMD-vol. 235, pp. 51–60.

Karandikar, P., Chou, T.-W., 1992. Characterization and modeling of microcracking and elastic moduli changes in nicalon-CAS composites. Compos. Sci. Technol. 46, 253–259.

Karbhari, V.M., Rydin, R.W., 1999. Impact characterization of RTM composites—II: damage mechanisms and damage evolution in plain weaves. J. Mater. Sci. 34, 5641–5648.

Lambros, J., Rosakis, A.J., 1995. Shear dominated transonic growth in a bimaterial—I. experimental observations.. J. Mech. Phys. Solids 43, 169–188.

Lambros, J., Rosakis, A.J., 1997. An experimental study of the dynamic delamination of thick fiber reinforced polymeric matrix composite laminates. Exp. Mech. 37, 360–366.

Lee, J.-W., Daniel, I.M., 1990. Progressive transverse cracking of crossply composite laminates. J. Compos. Mater. 24, 1225–1243.

Li, X., Carlsson, L.A., 1999. The tilted sandwich debond (TSD) specimen for face/core interface fracture characterization. J. Sandwich Struct. Mater. 1 (1), 65–75.

Mines, R.A.W., Roach, A.M., Jones, N., 1999. High velocity perforation behaviour of polymer composite laminates. Int. J. Impact Eng. 22, 561–588.

Needleman, A., Rosakis, A.J., 1999. The effect of bond strength and loading rate on the conditions governing the attainment of intersonic crack growth along interfaces. J. Mech. Phys. Solids 47, 2411–2449.

Oguni, K., Tan, C.Y., Ravichandran, G., 2000. Failure mode transition in unidirectional E-Glass/Vinylester composites under multiaxial compression. J. Compos. Mater. 34, 2081–2097.

Parameswaran, V., Shukla, A., 1998. Dynamic fracture of a functionally gradient material have discrete property variation. J. Mater. Sci. 33, 3303–3311.

Rajapakse, Y.D.S., 1995. Recent advances in composite research for marine structures. In: Allen, H.G. (Ed.), Sandwich Construction 3, Proceedings of the second international conference, vol. II. Chameleon Press Ltd., London, pp. 475–486.

Ravi-Chandar, K., Knauss, W.G., 1984. An experimental investigation into dynamic fracture: III. on steady-state crack propagation and crack branching. Int. J. Fract. 26, 141–154.

Riley, W.F., Dally, J.W., 1966. A photoelastic analysis of stress wave propagation in a layered model. Geophysics 31, 881–899.

Rosakis, A.J., Samudrala, O., Singh, R.P., Shukla, A., 1998. Intersonic crack propagation in bimaterial systems. J. Mech. Phys. Solids 46, 1789–1813.

Semenski, D., Rosakis, A.J., 1999. Dynamic crack initiation and growth in light-core sandwich composite materials. In: Proceedings of the 17th Danubia-Adria Symposium on Experimental Mechanics in Solid Mechanics, Prague, pp. 297–300.

Shenoy, V.B., Schwartzman, A.F., Freund, L.B., 2000. Crack patterns in brittle thin films. Int. J. Fract. 103, 1–7.

Singh, R.P., Shukla, A., 1996. Subsonic and intersonic crack growth along a bimaterial surface. J. Appl. Mech. 63, 919–924.

Sun, C.T., Rechak, S., 1988. Effect of adhesive layers on impact damage in composite laminates. In: Whitcomb, J.D. (Ed.), Composite Materials: Testing and Design (eighth conference). ASTM STP 972, American Society for Testing and Materials, Philadelphia, pp. 97–123.

Takeda, N., Sierakowski, R.L., Ross, C.A., Malvern, L.E., 1982. Delamination-crack propagation in ballistically impacted glass/epoxy composite laminates. Exp. Mech. 22, 19–65.

Valenti, M., 2001. Stealth on the water. ASME Mech. Eng. 123, 56–61.

Vinson, J.R., Sierakowski, R.L., 1986. The behavior of structures composed of composite materials. Martinus, Nijhoff Publishers, Dordrecht.

Vizzini, A.J., Lagace, P.A., 1987. The buckling of a delaminated sublaminate on an elastic foundation. J. Compos. Mater. 21, 1106–1117.

Walter, M.E., Ravichandran, G., 1997. Experimental simulation of matrix cracking and debonding in a model brittle matrix composite. Exp. Mech. 37, 130–135.

Wen, H.M., Reddy, T.Y., Reid, S.R., Soden, P.D., 1998. Indentation, penetration and perforation of composite laminates and sandwich panels under quasi-Static and projectile loading. Key Eng. Mater., 141–143, 501–552.

Williams, M.L., 1952. Stress singularities resulting from various boundary conditions in angular corners in extension. J. Appl. Mech. 19, 526–528.

Wu, H.T., Springer, G.S., 1988. Measurements of matrix cracking and delamination caused by impacted on composite plates. J. Compos. Mater. 22, 518–532.

Xu, L.R., Rosakis, A.J., 2002a. Impact failure characteristics of sandwich structures; part II: effects of impact speeds and interfacial bonding strengths. Int. J. Solids Struct. 39(16), 4237–4248.

Xu, L.R., Rosakis, A.J., 2002b. An experimental study on impact-induced failure events in homogeneous layered materials using dynamic photoelasticity and high-speed photography. Opt. Lasers Eng., in press.

Yu, C., Ortiz, M., Pandolfi, A., Rosakis, A., 2001. Private communications.